Design and Dynamics Modelling of a Novel Rotary Magnetic Microrobot

Ruhollah Khalesi [a], Hossein Nejat Pishkenari [b]* and Gholamreza Vossoughi [c]

[a] *Nanorobotics Laboratory, Department of Mechanical Engineering, Sharif University of Technology, Tehran, Iran – email: ro.khalesi@gmail.com ;*

[b] *Nanorobotics Laboratory, Department of Mechanical Engineering, Sharif University of Technology, Tehran, Iran – email: nejat@sharif.ir – mobile: 0912-262-83070;*

[c] *Department of Mechanical Engineering, Sharif University of Technology, Tehran, Iran – email: vossough@sharif.edu*

**Corresponding author: nejat@sharif.edu*

Abstract

Swimming microrobots with various applications in targeted drug delivery, diagnostics, and minimally invasive surgery, have attracted a lot of interest in recent years. They are usually steered by an external energy source such as a magnetic field. In this paper, we have proposed a novel low Reynolds number swimmer driven by a rotary magnetic field and discussed its design parameters. The microrobot consists of a central sphere and two arms, which create linear movement with its rotation. It is shown that the microrobot speed depends on its dimensions and the magnetic field angular velocity. In addition, we have shown simultaneous control of three microrobots based on their different reactions to the same input.

Keywords: microrobot; rotary magnetic field; non-homogeneous microrobot; low Reynolds number; simultaneous control

I. Introduction

Microrobots, or MRs, which are extremely small with dimensions on the micro-meter scale, find applications in diverse domains including micro-assembly and drug delivery [1-3]. Due to the compact nature of MRs, their usage of onboard sensors and actuators is quite infrequent. However, researchers have explored various MEMS-based techniques for enabling functionality in MRs, including electro-thermal, piezoelectric [4-6], and electromagnetic actuators. A comprehensive overview of relevant studies can be found in [7]. In [8], Zhang et al. introduced a micro-robot (MR) design featuring end-effectors. Their approach utilized a global magnetic field to control the position of the MR and enable gripper grasping and releasing commands. Another MR model called Quadroar was proposed by Jalali et al.[9]. Quadroar was equipped with one linear and four rotary actuators, allowing movement in forward and transverse directions as well as three-dimensional reorientation. The theoretical findings were experimentally verified using a mm-scale Quadroar in [10]. Furthermore, some research works have

presented MRs with both linear and rotary actuators, along with proposed strategies for position control [4, 11]. However, these MR designs cannot currently be manufactured on a micro-meter scale due to technological limitations.

Using external energy sources as an actuation signal is a more practical solution. Various mechanisms, including electrics, acoustics, magnetic fields, thermal energy, and light, are utilized for actuating MRs [12-14]. Among these options, the use of a magnetic field is widely preferred due to its ability to penetrate different materials without causing damage while swiftly generating force and torque. Magnetic fields can be utilized in different modes, such as rotating fields [15], oscillating fields [16], and field gradients [17, 18].

As an example, Khalesi et al. [16] introduced a MR design comprising a rotatable disk-equipped cilium capable of achieving a maximum speed of 520 µm/s. The MR's motion is governed by a stepping magnetic field. Khalil et al. [19], proposed a sperm-like MR, where the MR possesses a magnetic head and moves with an average speed of 160 µm/s under the influence of an external oscillating magnetic field. The researchers also conducted experimental tests to validate the controllability and steering of the MR. Additionally, other studies have concentrated on developing control strategies specifically for single MRs. To this end, various approaches such as optimal control [20] and neuro-fuzzy network [21] have been employed.

Integrating multiple robots can enhance the speed and functionality of a system [22]. There are two main methods for controlling multiple magnetic MRs. The first method involves creating different magnetic fields in the workspace to exert distinct forces on each MR. Sitti et al. controlled two MRs using electrostatic anchoring pads [23]. The presented method requires special surfaces and is limited to 2D movements. Control of identical MRs is also challenging. Kumar et al. proposed a force control method based

on varying gradients and stationary electromagnetic coils for two MRs [24]. The results obtained from numerical simulations were validated through macro-scale experiments. Simultaneous and independent control of two MRs in three-dimensional space was achieved by Misra et al., who presented an electromagnetic setup consisting of nine electromagnetic coils [25]. Another approach proposed in [26] involved controlling the position of multiple MRs using a magnetic field gradient. Rotating permanent magnets were utilized to exert the desired forces. However, due to the small distances between MRs, generating separate fields at each robot location is challenging [27].

The second method utilizes non-identical MRs with different magnetic, geometric, electric, or thermal properties. These MRs are controlled independently by uniform magnetic fields [28]. Special attention needs to be given in the design process of this method to ensure that MRs can produce varying outputs despite receiving similar inputs. Diller et al. demonstrated the simultaneous control of MRs with different geometric properties (termed mag-Bots) in 2D [29]. Nelson et al. manipulated micro-objects using two helical MRs controlled by a rotating magnetic field [30]. Cheang et al. controlled magnetically different MRs by adjusting the strength and frequency of a rotating magnetic field [31].

Controlling non-identical robots is simpler, but needs special devices and sophisticated designs. In this study, we have introduced an innovative design (Figure 1) for simultaneously controlling multiple MRs, each consisting of a sphere and two arms with an attached disk. By applying an external rotating magnetic field, the MRs rotate and move via drag force. We have analytically calculated the relationship between linear and angular velocities, explored the impact of physical and magnetic properties on MR speed, and demonstrated the simultaneous control of three MRs through simulation.

In the following section, the dynamic equations are written in general. In section three, the effects of various physical and magnetic parameters on the MR velocity are examined through simulations performed. In the fourth section, the simultaneous and independent control of two MRs is theoretically investigated.

[figure 1]

II. Equation of motion

The Reynolds number, a measure of the balance between inertial and viscous forces, is significantly low in MRs because of their reduced size and slow movement. As a result, the contribution of inertial forces can be considered negligible, and the viscous forces are dominant. Thus, Stokes equations can be derived from Navier-Stokes equations as follow [32]

$$\nabla \boldsymbol{p} = \mu \nabla^2 \boldsymbol{u}, \nabla \boldsymbol{u} = 0 \quad (1)$$

In this equation, $\boldsymbol{p}$ and $\boldsymbol{u}$ are pressure and the fluid velocity vectors, and μ is the dynamic viscosity of the fluid. Magnetic force ($\boldsymbol{F_m}$) and torques ($\boldsymbol{\tau_m}$) can be calculated using these equations:

$$\boldsymbol{F_m} = (\boldsymbol{m}.\nabla)\boldsymbol{B} \quad (2)$$

$$\boldsymbol{\tau_m} = \boldsymbol{m} \times \boldsymbol{B} \quad (3)$$

where $\boldsymbol{m}$ is MR magnetic dipole moment, and $\boldsymbol{B}$ is the external magnetic field. The MR moves in fluid so another force and torque applied to the MR is the drag force [33, 34].

$$\boldsymbol{F_{drag}} = -\mu[\boldsymbol{K}]\boldsymbol{u} \quad (4)$$

$$\boldsymbol{\tau_{drag}} = -\mu[\boldsymbol{Q}]\boldsymbol{\omega} \quad (5)$$

In these equations, $\boldsymbol{u}$, $\boldsymbol{F_{drag}}$, $\boldsymbol{\omega}$, and $\boldsymbol{\tau_{drag}}$ are relative velocity, drag force, angular velocity, and drag torque. $\boldsymbol{Q}$ and $\boldsymbol{K}$ are drag force and torque coefficient matrices. Figure 2 shows the applied forces and torques.

[figure 2]

If the MR rotates in the y-direction with a rotational speed Ω, the relative velocity of the disks in the z-direction will be equal to $(L+R+r)\Omega$. In the given equation, the variable L represents the length of the arm, while R and r stand for the radii of the sphere and disk respectively. The disk's movement will exert a force in the y-direction and a torque against the applied external magnetic torque. As a result of this force, the MR will move in the y-direction with the speed of V_{lin}. Due to the MR's movement, a drag force opposite to the y-direction and a drag torque in the same direction as the magnetic torque are exerted. Moreover, the movement of the middle sphere will produce a drag force in the opposite direction of y and a torque opposite to the external one. The equations of motion are as follows:

$$\sum \boldsymbol{F} = m\boldsymbol{a} \rightarrow m\ddot{y} = F^{y}_{MBD\_rot} + F^{y}_{MBD\_lin} + F^{y}_{MBS\_lin} \quad (6)$$

$$\sum \boldsymbol{T} = \boldsymbol{I\alpha} \rightarrow I_{yy}\ddot{\phi} = T^{y}_{MBD\_rot} + T^{y}_{MBD\_lin} + T^{y}_{D\_rot} + T^{y}_{S\_rot} + T^{y}_{external} \quad (7)$$

In Eq. (6), $F^{y}_{MBD\_rot}$, $F^{y}_{MBD\_lin}$, and $F^{y}_{MBS\_lin}$ are the force applied to the MR by rotational and linear movement of the disks, and linear movement of the sphere respectively. In Eq. (7) $T^{y}_{MBD\_rot}$, $T^{y}_{MBD\_lin}$, $T^{y}_{D\_rot}$, $T^{y}_{S\_rot}$, and $T^{y}_{external}$ are the torque exerted to the MR by rotational and linear movement of the disks, the disks, and the sphere drag torque, and the external magnetic torque. Forces and torques in the y direction are effective in the movement and in other directions Forces and Torques are simplified due to symmetry.

If the right side of Eq. (7) becomes zero, the rotational movement of the MR becomes stable. By applying a rotating external field, the MR also starts to rotate with a certain angle difference from the external field. The value of this angle difference can be calculated from the combination of Eq. (6) and (7). By solving these equations, the

speed and angle between the direction of the external magnetic field and the MR arm (α) can be determined as follows according to the parameters of the MR:

$$\Omega = -\frac{3}{8}\left(mB\sin(\alpha)\left(8r\cos(2\theta)-9R\pi-40r\right)\right)/A \tag{8}$$

$$V_{lin} = 3r\left(R+r+L\right)mB\sin(\alpha)\sin(2\theta)/A \tag{9}$$

$$A = \mu\left(6\cos(2\theta)\pi Rr\left(3\left(L^2+2\left(RL+rL+Rr\right)\right)+3r^2-R^2\right)-64\cos(2\theta)r^4+\right. \tag{10}$$
$$180\pi Rr\left(RL+rL+Rr\right)+768r^2\left(RL+rL+Rr\right)+384r^2\left(L^2+R^2\right)+27R^4\pi^2+$$
$$\left.90\pi L^2Rrr+210\pi R^3r+162\pi Rr^3+704r^4\right)$$

Here, θ is half of the relative angle between disks. Knowing the rotation speed of the field, Ω, it is possible to obtain the value of α from Eq. (8) and calculate the linear velocity, V_{lin}, by inserting it into Eq. (9).

III. Numerical Simulation

We have conducted some numerical simulations to demonstrate the performance of the proposed MR and sensitivity analysis. MR design parameters are shown in Table 1. The fluid viscosity is $0.001\,\mathrm{m}^2/\mathrm{s}$ and the external magnetic field strength is $0.2mT$.

[table 1]

As seen in Equations (6) and (7), the linear velocity of the microrobot is affected by multiple forces and torques. Each of them is dependent on the microrobot's geometric or physical properties, as well as the properties of the magnetic field. Figure 3 demonstrates how MR linear velocity varies with MR geometrical parameters. Except for the indicated parameter, the other MR geometrical specification is the same as in Table 1. Increasing the disk's angle reduces the resulting drag torque and slows the angular velocity. But after this parameter passes 45°, the effective drag force and MR's linear velocity decrease. Increasing the length of arms and the radius of disks has a dual effect. As the first effect, as these parameters increase, drag torque increases and

angular velocity decreases, resulting in a decrease in linear velocity. However, as the second effect, because the MR's motion mechanism also relies on the drag from the disks, increasing these parameters leads to an increase in the linear velocity. In the initial portion of the plot, where $l < 975\ \mu$m and $r < 425\ \mu$m, the first effect appears to play a stronger role, while the second effect gains dominance in the subsequent half. By increasing the sphere's radius, the drag torque will increase, and angular and linear velocity will reduce. The change in the slope of the velocity graph in this figure is due to crossing the threshold of the achievable velocity for the MR.

[figure 3]

To evaluate the dynamic response of the MR, a 100s simulation with different magnetic field angular velocities has been conducted. In these simulations, a rotating magnetic field with angular velocities of 40, 65, 75, and $100^\circ/s$ is applied in the y -direction. Linear and angular velocities of the MR are shown in Figure 4 and Figure 5. As can be seen in Figure 4, there is a threshold for MRs angular velocity. If the external magnetic field rotation speed exceeds this threshold, the MR cannot rotate with the necessary angular velocity due to the presence of significant drag torque. Therefore, the angle between its magnetization vector and the external magnetic field increases. Once this angle surpasses 180 degrees, the MR rotates in the opposite direction, resulting in negative velocity, and the total displacement of the MR will be reduced (Figure 5). For this MR, the limit is about $67^\circ/s$.

[figure 4]

[Figure 5]

Table 2 shows the mean linear and angular velocity of the MR in different conditions. Figure 6 illustrates the linear velocity of two different MRs versus external magnetic

field angular velocity. MRs parameters are the same as in Table 1, except for the values shown in the legend. The possibility to achieve different linear velocities by the same input is a base of simultaneous control. In the first part of this figure, the first MR moves slower and in the second part, it moves faster. So, these MRs can be controlled simultaneously with a control strategy stated in our previous work [16]. Also, by adding a mechanism like the one used in [9] for rotating disks, it will be possible to fix multiple MRs and displace a special one.

[table 2]

[figure 6]

IV. Simultaneous control

In this section, we use the possibility of generating different velocities via the same magnetic field to individually control geometrically non-homogenous MRs. The focus is on controlling two MRs simultaneously, but the concept is similar for more MRs. Figure 6 shows the average velocity of the MRs versus the external magnetic field rotation frequency for the two MRs. We can see that these MRs respond differently to similar inputs, and the operator can choose the suitable frequency regarding the MRs' current and desired position. Since the values of this ratio are limited, each displacement must divide into two parts and combine the moves to get the final desired displacement.

Figure 7 and Figure 8 show the control input and MRs' trajectory. In the conducted simulation, MRs move from [0,1,0] and [1,0,3] millimeters to [7, 11, 15] and [10, 13, 3] millimeters. For this purpose, in the first step, an external magnetic field for 87.2 and 15.3s respectively with angular velocities of 50 and 65 $^{\circ}/s$ is applied in the x-direction to compensate for this axis position error. Then y-direction error was compensated by a magnetic field with angular velocities of 45 and 51.3 $^{\circ}/s$ for 97 and 8.3s respectively. The final step is applying a magnetic field in the z-direction for 106.4 and 195.3s

respectively with angular velocities of 50 and 65 $^{\circ}/s$. Simultaneous control of more MRs with similar concepts requires increasing the number of moving parts in each direction.

[figure 7]

[figure 8]

V. conclusion

In this paper, we presented a novel magnetic swimming microrobot (MR), actuated by external rotating magnetic fields. The MR consists of a sphere, with two arms, and a disk is attached at the end of each arm. The disks are perpendicular to each other, and the unalignment is the main cause of the drag forces and the movement. When an external magnetic field is applied, the MR rotates to be aligned with the external magnetic field vector. By increasing the field rotation velocity, MR's angular and linear velocity increase too, but from a specific value, the MR starts to rotate in the opposite direction which reduces its average velocity. Using the derived analytical formula for the velocity of the MR, design parameters like the radius of the sphere and disk, and the length of the arms were studied to determine how they affect MR's speed. We also studied two MRs with different properties and demonstrated the simultaneous control of these MRs based on their different responses to the same input.

References

[1] Lee, H., Choi, H., Lee, M. *et al*., "Preliminary study on alginate/NIPAM hydrogel-based soft microrobot for controlled drug delivery using electromagnetic actuation and near-infrared stimulus," *Biomedical Microdevices*, 20(4), pp. 1-9 (2018), doi: 10.1007/s10544-018-0344-y.

[2] Nadafi Db, R., Nazari Nejad, S., Kabganian, M. *et al*., "Adaptive control of a legged capsular microrobot based on Lyapunov stability criteria," *Proceedings of the Institution of Mechanical Engineers, Part C: Journal of Mechanical Engineering Science*, 226(4), pp. 887-899 (2011), doi: 10.1177/0954406211417940.

[3] Chao, G., Bo, P., Guojun, N. *et al*., "Modeling and design optimization of master manipulator for robot-assisted minimally invasive surgery," *Proceedings of the*

Institution of Mechanical Engineers, Part C: Journal of Mechanical Engineering Science, 237(7), pp. 1537-1549 (2022), doi: 10.1177/09544062221128695.

[4] Nejat Pishkenari, H. and Mohebalhojeh, M., "Optimal motion control of three-sphere based low-Reynolds number swimming microrobot," *Robotica*, 40(5), pp. 1257-1273 (2022), doi: 10.1017/S0263574721000953.

[5] Zhao, Q., Chen, J., Zhang, H. *et al.*, "Hydrodynamics modeling of a piezoelectric micro-robotic fish with double caudal fins," *Journal of Mechanisms and Robotics*, 14(3), p. 034502 (2022), doi: 10.1115/1.4052973.

[6] Jiang, J., Yang, Z., Ferreira, A. *et al.*, "Control and autonomy of microrobots: Recent progress and perspective," *Advanced Intelligent Systems*, 4(5), p. 2100279 (2022), doi: 10.1002/aisy.202100279.

[7] Yang, S. and Xu, Q., "A review on actuation and sensing techniques for MEMS-based microgrippers," *Journal of Micro-Bio Robotics*, 13(1-4), pp. 1-14 (2017), doi: 10.1007/s12213-017-0098-2.

[8] Zhang, J., Salehizadeh, M. and Diller, E., "Parallel pick and place using two independent untethered mobile magnetic microgrippers," in *2018 IEEE International Conference on Robotics and Automation (ICRA)*, pp. 123-128 (2018), doi: 10.1109/ICRA.2018.8462861.

[9] Jalali, M. A., Alam, M.-R. and Mousavi, S., "Versatile low-Reynolds-number swimmer with three-dimensional maneuverability," *Physical Review E*, 90(5), p. 053006 (2014), doi: 10.1103/PhysRevE.90.053006.

[10] Saadat, M., Mirzakhanloo, M., Shen, J. *et al.*, "The Experimental Realization of an Artificial Low-Reynolds-Number Swimmer with Three-Dimensional Maneuverability," *2019 American Control Conference (ACC)*, pp. 4478-4484 (2019), doi: 10.23919/ACC.2019.8814346.

[11] Esfandbod, A., Nejat Pishkenari, H. and Meghdari, A., "Dynamics and Control of a Novel Microrobot with High Maneuverability," *Robotica*, 39(10), pp. 1729-1738 (2021), doi: 10.1017/S0263574720001460.

[12] Halder, A. and Sun, Y., "Biocompatible propulsion for biomedical micro/nano robotics," *Biosensors and Bioelectronics*, p. 111334 (2019), doi: 10.1016/j.bios.2019.111334.

[13] Qu, C., Pei, Y.-C., Xin, Q.-Y. *et al.*, "A reciprocating permanent magnetic actuator for driving magnetic micro robots in fluids," *Proceedings of the Institution of Mechanical Engineers, Part C: Journal of Mechanical Engineering Science*, 235(22), pp. 6451-6462 (2021), doi: 10.1177/09544062211014547.

[14] Sayyaadi, H. and Bahmanyar, S., "Development of a new mechanism to change velocity in a helical swimmer robot at low Reynolds number," *Scientia Iranica. Transaction B, Mechanical Engineering*, 25(5), pp. 2616-2627 (2018), doi: 10.24200/SCI.2018.20031.

[15] Mahoney, A. W., Sarrazin, J. C., Bamberg, E. *et al.*, "Velocity Control with Gravity Compensation for Magnetic Helical Microswimmers," *Advanced Robotics*, 25(8), pp. 1007-1028 (2011), doi: 10.1163/016918611X568620.

[16] Khalesi, R., Nejat Pishkenari, H. and Vossoughi, G., "Independent control of multiple magnetic microrobots: design, dynamic modelling, and control," *Journal of Micro-Bio Robotics*, pp. 1-10 (2020), doi: 10.1007/s12213-020-00136-1.

[17] Peyer, K. E., Zhang, L. and Nelson, B. J., "Bio-inspired magnetic swimming microrobots for biomedical applications," *Nanoscale*, 5(4), pp. 1259-1272 (2013), doi: 10.1039/C2NR32554C.

[18] Belharet, K., Folio, D. and Ferreira, A., "Three-Dimensional Controlled Motion of a Microrobot using Magnetic Gradients," *Advanced Robotics*, 25(8), pp. 1069-1083 (2011), doi: 10.1163/016918611X568657.

[19] Khalil, I. S., Dijkslag, H. C., Abelmann, L. *et al.*, "MagnetoSperm: A microrobot that navigates using weak magnetic fields," *Applied Physics Letters*, 104(22), p. 223701 (2014), doi: 10.1063/1.4880035.

[20] Nickandish, A. and Nejat Pishkenari, H., "Dynamic Modeling and Optimal Control of a Novel Microswimmer with Gimbal Based Disks," *Robotica*, 39(8), pp. 1468-1484 (2021), doi: 10.1017/S0263574720001289.

[21] Salehi, M., Nejat Pishkenari, H. and Zohoor, H., "Position control of a wheel-based miniature magnetic robot using neuro-fuzzy network," *Robotica*, pp. 1-16 (2022), doi: 10.1017/S0263574722000662.

[22] Mao, L., Li, Z., Zhang D. *et al.*, "A distributed market-based boundary coverage algorithm for multiple microrobots with network connectivity maintenance," *Advanced Robotics*, 27(17), pp. 1361-1373 (2013), doi: 10.1080/01691864.2013.826422.

[23] Pawashe, C., Floyd, S. and Sitti, M., "Multiple magnetic microrobot control using electrostatic anchoring," *Applied Physics Letters*, 94(16), p. 164108 (2009), doi: 10.1063/1.3123231.

[24] Wong, D., Steager, E. B. and Kumar, V., "Independent control of identical magnetic robots in a plane," *IEEE Robotics and Automation Letters*, 1(1), pp. 554-561 (2016), doi: 10.1109/LRA.2016.2522999.

[25] Ongaro, F., Pane, S., Scheggi, S. *et al.*, "Design of an Electromagnetic Setup for Independent Three-Dimensional Control of Pairs of Identical and Nonidentical Microrobots," *IEEE transactions on robotics*, 35(1), pp. 174-183 (2018), doi: 10.1109/TRO.2018.2875393.

[26] Khalesi, R., Yousefi, M., Nejat Pishkenari, H. *et al.*, "Robust independent and simultaneous position control of multiple magnetic microrobots by sliding mode controller," *Mechatronics*, 84, p. 102776 (2022), doi: 10.1016/j.mechatronics.2022.102776.

[27] Chen, X. Z., Jang, B., Ahmed, D. *et al.*, "Small‐Scale Machines Driven by External Power Sources," *Advanced Materials*, 30(15), p. 1705061 (2018), doi: 10.1002/adma.201705061.

[28] Chowdhury, S., Jing, W. and Cappelleri, D. J., "Controlling multiple microrobots: recent progress and future challenges," *Journal of Micro-Bio Robotics*, 10(1-4), pp. 1-11 (2015), doi: 10.1007/s12213-015-0083-6.

[29] Diller, E., Floyd, S., Pawashe, C. *et al.*, "Control of multiple heterogeneous magnetic microrobots in two dimensions on nonspecialized surfaces," *IEEE Transactions on Robotics*, 28(1), pp. 172-182 (2011), doi: 10.1109/TRO.2011.2170330.

[30] Huang, T.-Y., Qiu, F., Tung, H.W. *et al.*, "Cooperative manipulation and transport of microobjects using multiple helical microcarriers," *Rsc Advances*, 4(51), pp. 26771-26776 (2014), doi: 10.1039/C4RA02260B.

[31] Kei Cheang, U., Lee, K., Julius, A. A. *et al.*, "Multiple-robot drug delivery strategy through coordinated teams of microswimmers," *Applied physics letters*, 105(8), p. 083705 (2014), doi: 10.1063/1.4893695.

[32] Ghanbari, A., Bahrami, M. and Nobari, M., "Methodology for artificial microswimming using magnetic actuation," *Physical Review E*, 83(4), p. 046301 (2011), doi: 10.1103/PhysRevE.83.046301.

[33] Mirzakhanloo, M., Jalali, M. A. and Alam, M.-R., "Hydrodynamic choreographies of microswimmers," *Scientific reports*, 8(1), p. 3670 (2018), doi: 10.1038/s41598-018-21832-w.

[34] Jafar, K., Hadi, and Peiman, N., "Adaptive neural dynamic surface control for uniform energy exploitation of floating wind turbine," *Applied Energy*, 316, p. 119132 (2022), doi: 10.1016/j.apenergy.2022.119132.

Figures

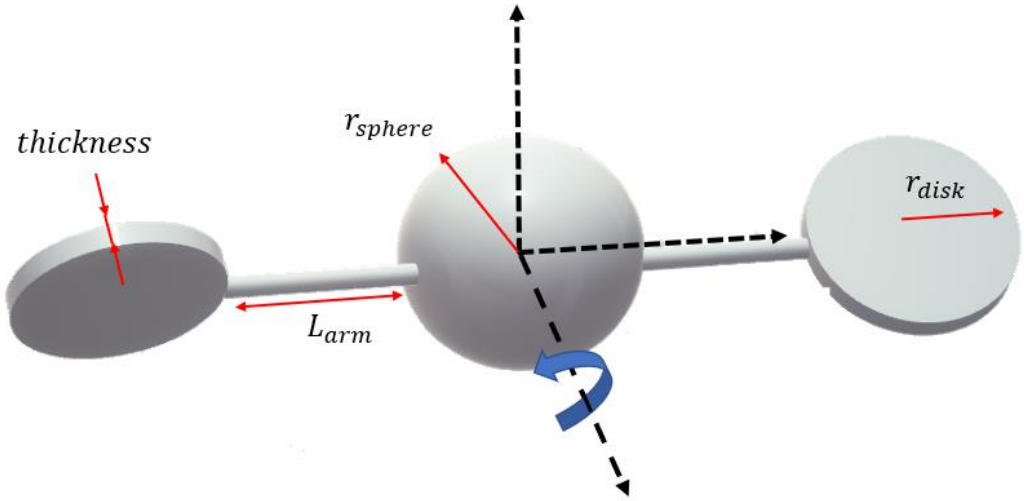

Figure 1 Front and side views of MR, consist of a sphere with radius R and thickness t, disks with radius r, and arms with length L

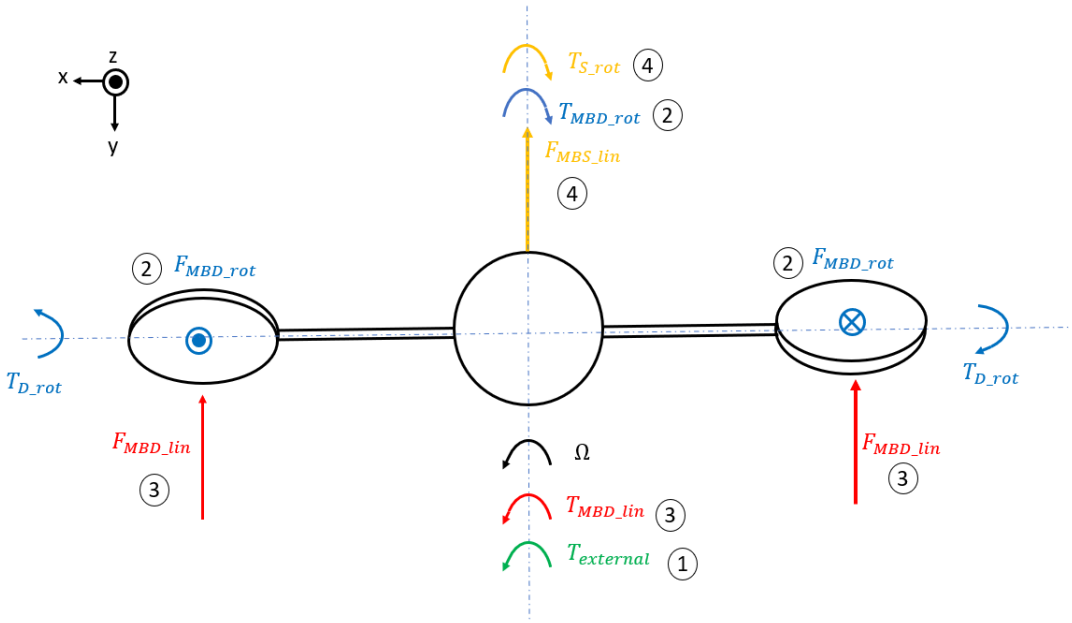

Figure 2 The applied forces and torques.

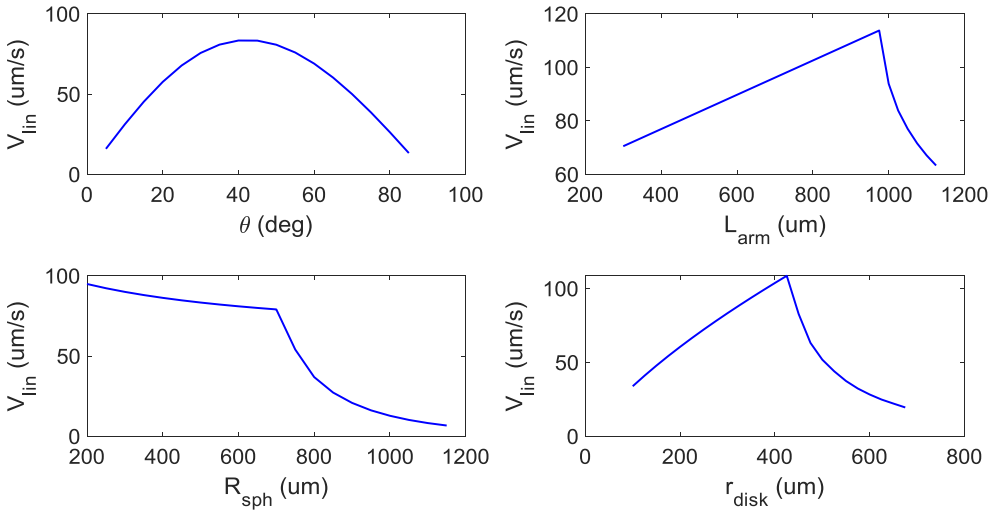

Figure 3 Linear velocity of the MR versus disks angles, length of arms, sphere, and disks radius

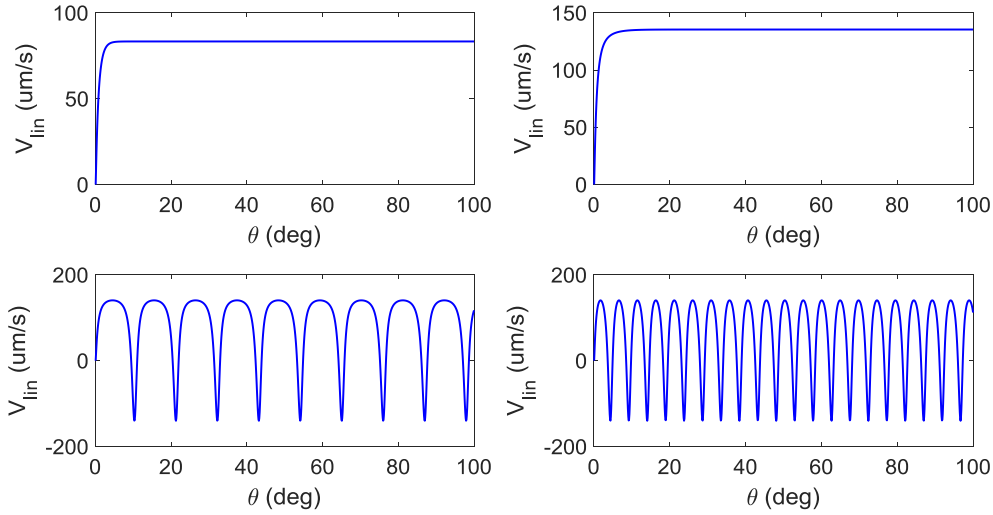

Figure 4 MR linear velocity in the different rotation speeds of the external magnetic field.

a) $\omega_{ext} = 40\,^{\circ}/_{s}$ b) $\omega_{ext} = 65\,^{\circ}/_{s}$ c) $\omega_{ext} = 75\,^{\circ}/_{s}$ d) $\omega_{ext} = 100\,^{\circ}/_{s}$

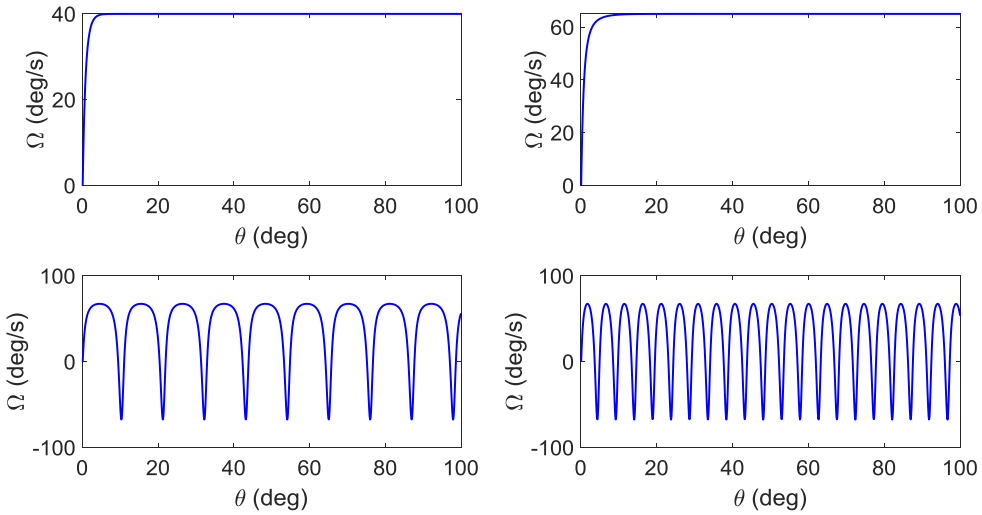

Figure 5 MR angular velocity in the different rotation speeds of the external magnetic field.

a) $\omega_{ext} = 40\,^{\circ}/_{s}$ b) $\omega_{ext} = 65\,^{\circ}/_{s}$ c) $\omega_{ext} = 75\,^{\circ}/_{s}$ d) $\omega_{ext} = 100\,^{\circ}/_{s}$

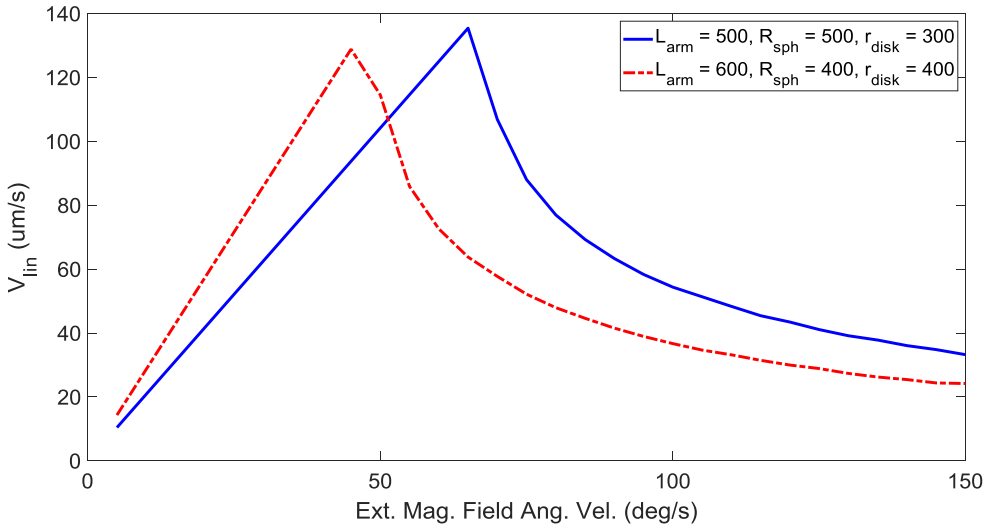

Figure 6 Linear velocity of two different MRs versus external magnetic field angular velocity

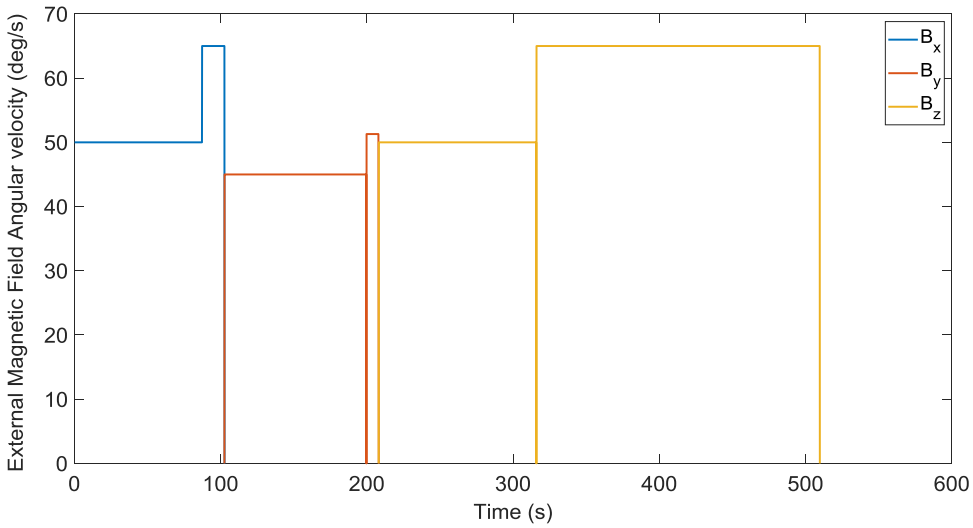

Figure 7 External magnetic field angular velocity for 3d simultaneous control of two MRs

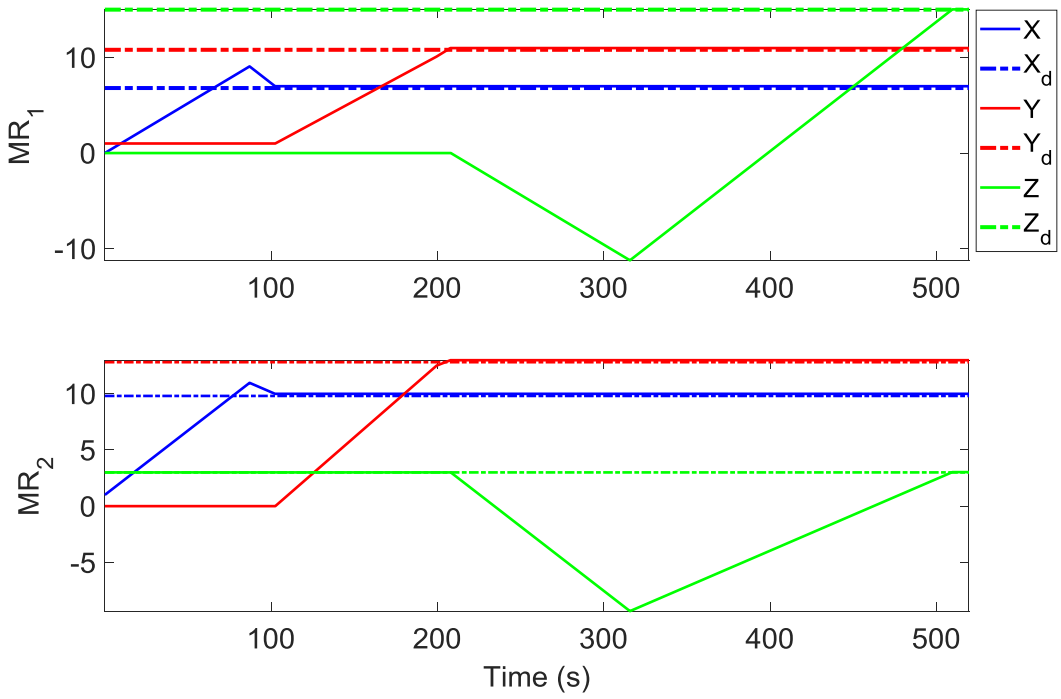

Figure 8 MRs position in 3d simultaneous control of two MRs

Tables

Table 1 MR specifications

parameter	unit	Value
Radius of sphere	μm	500
Radius of disks	μm	300
Length of Arms	nm	500
Thickness	μm	20
Angle of disks	deg	45
MR magnetization	Am^2	1e-7

Table 2 Mean linear and angular velocity of the MR

External magnetic field angular velocity $(^{\circ}/s)$	average angular velocity of the MR $(^{\circ}/s)$	average linear velocity of the MR $(\mu m/s)$
45.0	45.0	82.3
65.0	65.0	135.4
75.0	42.2	87.9
100.0	26.0	54.1

Brief Technical Biography:

Ruhollah Khalesi

received his B.Sc., M.Sc. and Ph.D. degrees in Mechanical Engineering from the Sharif University of Technology in 2012, 2014, and 2022 respectively. His-current research interests include Control and Robotics.

Hossein Nejat Pishkenari

earned his B.Sc., M.Sc. and Ph.D. degrees in Mechanical Engineering from the Sharif university of Technology in 2003, 2005 and 2010, respectively. Then he joined the Department of Mechanical Engineering at the Sharif University of Technology in 2012. Currently, he is directing the Nanorobotics Laboratory. One of his main research interests is Dynamics and Control of Micro/Nano Robots.

Gholamreza Vossoughi

received his Ph.D. from Mechanical Engineering Dept. at University of Minnesota in 1992. Ever since he has been a faculty member of Mechanical Engineering Dept. at Sharif University of Technology. He has served as the Manufacturing Engineering and Applied Mechanics Division Directors from 1994 to 1998 and as the Graduate Dean of the Mechanical Engineering from 1999 to 2003.

Statements and Declarations

Author Contributions: Conceptualization, methodology, software, and validation, R. Khalesi, and H. Nejat Pishkenari; formal analysis, and writing original draft preparation, R. Khalesi; writing review and editing, H. Nejat Pishkenari; supervision, Gh. Vossughi. All authors have read and agreed to the published version of the manuscript.

Funding: This research received no external funding

Data Availability Statement: The data presented in this study are available on request from the corresponding author.

Conflicts of Interest: The authors declare no conflict of interest